PERIODICA POLYTECHNICA SER. MECH. ENG. VOL. 45, NO. 2, PP. 201–216 (2001)

NON-FREE VORTEX FLOW EFFECTS IN AN AXIAL FLOW ROTOR

János VAD*[1], Ferenc BENCZE*, Alessandro CORSINI** and Franco RISPOLI**

*Department of Fluid Mechanics
Budapest University of Technology and Economics
Bertalan Lajos u. 4–6.
H–1111 Budapest, Hungary
Tel: (+36-1) 463-4072, Fax: (+36-1) 463-3464
e-mail: vad@simba.ara.bme.hu
** Department of Mechanics and Aeronautics
University of Rome 'La Sapienza'
Via Eudossiana 18
I–00184 Roma, Italia
Tel: (+39-6) 445 85233, Fax: (+39-6) 488 1759
e-mail: rispoli@dma.ing.uniromal.it

Received: 4 October, 1999

Abstract

This paper presents the analysis of three-dimensional flow field developing through an industrial axial flow fan rotor of non-free vortex design carried out on the basis of concerted experimental and numerical investigations. The paper focuses on non-free vortex flow effects requiring consideration in rotor blade design theories. The distortion of stream surfaces through the blading has been observed and a quantitative analysis of its effects on the blade loading condition has been carried out in the through-flow core region. The streamlines close to the blades have been modelled fitting to outward and inward conical stream tubes on the blade suction and pressure sides, respectively – termed 'cone couple model'. It has been pointed out that the blade lift can be satisfactorily described at midspan on the basis of the cone couple model, with use of pitch-averaged flow data. The loading aspects of the tested axial rotor have been discussed on the basis of both the pressure distribution in the vicinity of the blades and pitch-averaged flow data obtained upstream and downstream of the rotor. Sample calculations suggested that separate optimisation of the blade suction and pressure sides is essential if the three-dimensional blade-to-blade flow is intended to be considered in NFV fan design with use of two-dimensional cascade data.

Keywords: axial flow fans, laser Doppler anemometry, computational fluid dynamics, non-free vortex design, turbomachinery design aspects.

1. Introduction

If high average total head rise is to be achieved with a single stage fan of relatively low blade number, rotor speed and hub-to-casing ratio, the non-free vortex axial fan rotor design method (abbr. NFV method) can be applied in which a spanwise

[1]Corresponding author

increasing ideal total head rise is prescribed. The spanwise gradient in ideal total head rise results in characteristic three-dimensional (3D) secondary flow filling the dominant rotor blade passage flow region, as pointed out in experiments by e.g. DRING et al. [5] and VAD and BENCZE [20].

The appearance of radial velocity components in the rotor flow necessitates a consideration when choosing a method for design of NFV axial flow rotors. In the simplest design method, the radial flow is neglected and thus, cylindrical stream tubes are assumed through the rotor (e.g. WALLIS [23]). In such cases, the cylindrical section of the rotor fitting to one hypothetical stream tube is considered as a rectilinear cascade of infinite number of blades. For design procedures in which the radial velocity is not neglected but the through flow is modelled with use of conical stream surfaces, the blading enclosed in a stream tube can be developed again into a two-dimensional (2D) cascade plane. Such quasi-3D approach can employ passage-averaged equations for the flow properties varying from blade to blade along several surfaces (e.g. HORLOCK and MARSH [9]). In the most sophisticated computational design methodology overviewed in LAKSHMINARAYANA [11], the true 3D blade-to-blade flow is considered on the basis of Computational Fluid Dynamics (CFD). Such methodology usually involves less complex flow models for a preliminary optimisation of blading geometry. Once the blade-to-blade flow is assumed for several stream surface segments, classic 2D stationary cascade measurement data (e.g. HOWELL [8]) or cascade theories or CFD techniques help the designer to optimise the rotor geometry.

The above overview illustrates that 3D rotor flow effects can be considered in axial flow turbomachinery design on different levels of complexity. For instance, in the case of aircraft jet propulsion engines or power plant units, the required high efficiency and high reliability in performance account for application of the highest level 3D design. Due to the complex optimisation method, the resultant blade geometry may be rather complicated, leading to high expenses in manufacturing of such turbomachinery blades. Contrarily, for industrial ventilating fans a relatively simple blade geometry is required to minimise manufacturing costs and also to make possible modifications of blade stagger as appropriate. Nevertheless, an effectual and accurate design method for an industrial ventilating fan ensuring high efficiency is still desirable, although not as crucial as for the examples above. (However, if e.g. the ventilation system of a long distance transport tunnel is considered for which the electric power demand is in the order of magnitude of 1 MW, the rational use of electric power by means of efficiency improvement of the comprised axial fans is an important point of economics.) For such a reason, it is beneficial to elaborate a simplified but satisfactory 3D model for the NFV fan rotor flow. This model should serve as a basis for improved fan design in which 2D cascade data are utilised further on and simple cascade geometry can be obtained.

The paper reports a case study on a NFV axial fan rotor originally designed on the basis of 2D cascade data presented by HOWELL [8]. The applied design technique neglected the radial velocity components (SOMLYÓDY [15]). In contrast, the realised blade-to-blade flow showed 3D characteristics appearing as a torsion of interblade stream surface segments, as demonstrated in the experimental work

carried out by VAD and BENCZE [20] and in the numerical simulation of rotor flow physics reported in VAD et al. [18]. Based on such a state of art, this paper presents a simplified model for the 3D blade-to-blade flow developing in the rotor that is based on the numerical simulation of rotor flow described in CORSINI et al. [4]. With the use of the model, loading aspects of the blading are discussed, as a step to establish guidelines for the improvement in design through consideration of 3D blade-to-blade flow effects. The case study was carried out in a concerted action of experimental and CFD techniques (CORSINI et al. [4]).

2. Background

2.1. Experimental Apparatus and Procedure

The experimental investigation on the high performance fan was carried out in the axial flow fan facility at the Department of Fluid Mechanics, Technical University of Budapest. The measurements aimed the determination of global fan performance (characteristic and efficiency curves) and detailed laser Doppler anemometer (LDA) studies on the velocity field. The fan facility, its basic instrumentation, the related LDA measurement methodology and measurement error have been described in detail and further references are specified in VAD and BENCZE [21]. The NFV test fan rotor characteristics are: tip diameter 0.624 m, average tip clearance 3 mm, hub-to-casing ratio 0.676, $N = 12$ straight (unswept) circular arc plate blades, spanwise constant chord length of $\ell_0 = 171$ mm, design flow coefficient $\Phi_D = 0.5$. The fan performed a total head rise of $\Psi = 0.48$ at the design flow rate. The characteristic and efficiency curves of the test rotor (with stator) are presented in CORSINI et al. [4].

Table 1. Airfoil geometry of the test rotor

	Blade root	Midspan	Blade tip
R	0.676	0.833	0.990
Solidity	1.534	1.237	1.047
Camber radius/mm	360.7	425.5	493.1
Stagger/deg (from circumferential direction)	47.9	42.2	38.3

Data on the airfoil geometry are given in *Table 1*. Further details of the design method and test fan geometry can be found in VAD and BENCZE [20]. The fan was run at a speed of 1100 rpm. The Reynolds number (based on the airfoil chord length and relative inlet flow velocity at midspan) was $4 \cdot 10^5$.

3D LDA measurements have been carried out upstream and downstream of the rotor at a flow rate of Φ_D, with dismounted stator vanes. The velocity field upstream

and downstream of one selected blade passage was mapped from hub to tip, fitting to planes perpendicular to the rotor axis and located at $-0.06X$ (upstream of leading edges) and at $1.06X$ (downstream of trailing edges). For axial positions expressed as a portion of X, the axial co-ordinate is zero at the leading edge blade root and increases in the downstream direction. X is the axial chord at the hub. Processing and representation of LDA data is discussed e.g. in VAD and BENCZE [20].

2.2. Numerical Scheme

The numerical analysis of the axial flow rotor has been carried out adopting a self-developed finite-element Navier-Stokes code (BORELLO et al. [2]), (CORSINI et al. [4]). The code solves the steady and three-dimensional Reynolds averaged Navier-Stokes equations in a rotating frame. The adopted fluid dynamic closure is carried out with non-Newtonian stress-strain relationship in order to recover the anisotropy of the turbulent stress tensor (LAUNDER [12]). The Reynolds stress tensor is thus modelled in the form of a third order polynomial function of mean strain and vorticity tensors and of a non-linear scalar turbulent viscosity μ_t. The finite element formulation adopts a *Stabilised Petrov Galerkin Method*, modified for the application to 3D elements. The stabilisation technique involves a perturbation of the functions used to weight the advective-diffusive equations, acting as a discontinuous artificial contribution in the streamline direction (*Streamline Upwind Petrov Galerkin* term (BROOKS and HUGHES [3]; RISPOLI and SICILIANI [13]), and a perturbation of the continuity weights, acting as relaxation of incompressibility constraint proportional to a Laplacian pressure term (*Pressure Stabilised Petrov Galerkin* term (TEZDUYAR [17])). The resultant non-linear discrete system gives rise to a linearised Oseen-like problem, and is solved by a $GMRES$ based iterative solution procedure (SAAD and SCHULTZ [14]) (BORELLO et al. [2]).

2.3. Axial Flow Rotor Modelling

The computational domain, comprehending one blade passage and its tip clearance region and shown in *Fig. 1*, has been modelled using an H-type non-orthogonal body fitted grid (59 nodes streamwise, 21 nodes pitchwise and 31 nodes spanwise), adequately stretched toward solid boundaries in order to set the first grid node inside the inertial sublayer. The tip clearance geometry is approximated by 'pinching' the blade tip. Such simple approach, though it introduces a high skewing of the mesh in the clearance region, leads to easy implementation of tip gap boundary conditions (periodicity) and is suitable for simulating tip clearance flow behaviour providing good engineering approximation, see BASSON and LAKSHMINARAYANA [1], STORER and CUMPSTY [16], GOYAL and DAWES [6], CORSINI et al. [4].

The inlet boundary conditions were obtained from the inlet LDA velocity measurements (VAD et al. [19]), imposing the relative velocity field and an axi-

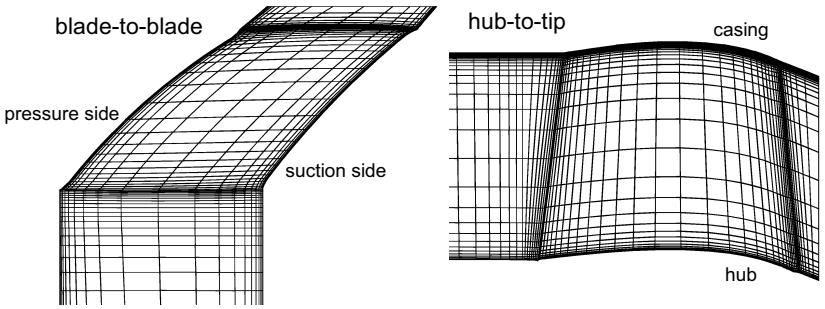

Fig. 1. Computational grid

symmetric turbulence intensity profile (VAD [18]) which account for the influence of inlet nose cone curvature and the rotor sucking effect near the tip flow region. The inlet profile of turbulence energy dissipation rate (ε) is based on the characteristic length scale definition (0.01 of rotor pitch at midspan) (HAH [7]; KUNZ and LAKSHMINARAYANA [10]). Furthermore in the outlet region Neumann conditions are specified, imposing homogeneous fluxes of turbulent variables and non-homogeneity for the static pressure. The near wall flow regions have been treated synthetically by the use of the logarithmic wall law modified to simulate the effect of the relative casing motion. Flow periodicity is strictly imposed at the permeable inlet and outlet boundary surfaces, and inside the tip clearance to ensure cyclic flow behaviour.

The present concerted scheme has already been applied to investigate the three-dimensional NFV rotor flow (CORSINI et al. [4]), (VAD et al. [18]). In these previous studies the validity of the numerical scheme has been assessed by comparing numerical results with the experimental ones. The pitch-averaged spanwise distribution of axial flow coefficient ($\varphi_3 = c_{3x}/u_C$) and ideal total head rise coefficient ($\psi_3 = 2R(c_{3u}/u_C)$) behind the rotor are shown in *Fig. 2*, demonstrating a fair agreement. The proposed Navier-Stokes technique is thus able to give correct prediction of the rotor flow behaviour with particular emphasis in the core region, with R ranging from 0.74 to 0.93.

3. Three-Dimensional Interblade Flow Aspects

The appearance of interblade radial flow components is unavoidable in a NFV rotor due to the presence of a spanwise blade circulation gradient. Contrarily the adopted design method relies on the classical assumption of cylindrical stream tubes through the rotor. Therefore the radial rearrangement of flow through the rotor (VAD et al. [18]) is implicitly neglected in design. *Figs. 3* and *4* show the velocity vector

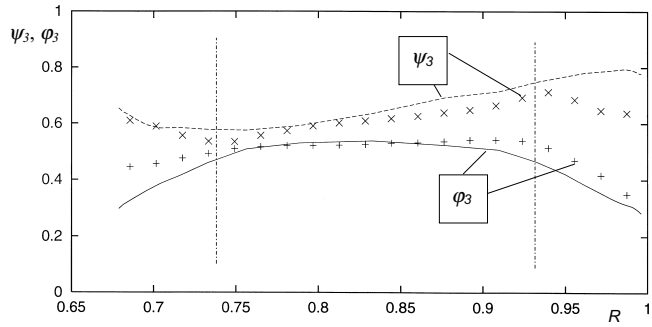

Fig. 2. Pitchwise averaged outflet flow data (symbols: measurements; lines: predictions)

plots in the vicinity of the blade surfaces approximately at the edge of the blade boundary layers. For these figures the blade geometry has been transformed into a rectangular region (according to the spanwise constant chord length). The abscissa (x) represents the length parameter along the chord, nondimensionalized by the chord length.

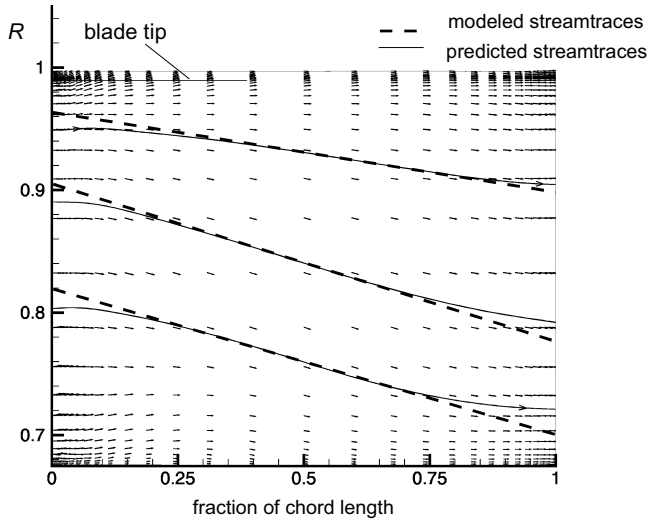

Fig. 3. Velocity field close to the blade pressure side

The computed stream traces have been mapped with reference to the following mid-chord spanwise position: in the vicinity of the hub $R = 0.76$, at mid span $R = 0.84$, in the vicinity of the tip $R = 0.93$.

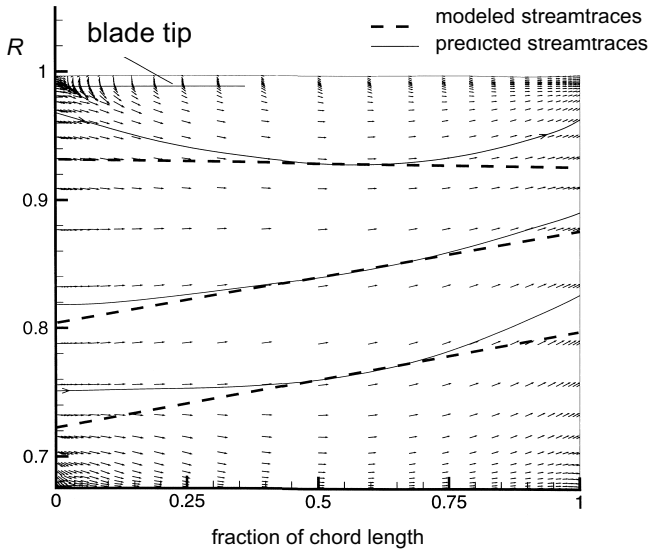

Fig. 4. Velocity field close to the blade suction side

The flow around the blade clearly shows a 3D behaviour resulting from the combination of secondary flow and end-wall effects (such as the leakage flow disturbance or the hub corner flow). *Figs. 3* and *4* suggest that torsion of incoming axisymmetric stream surfaces occurs within the blading. For the case study presented here, the torsion of interblade stream surface segments can be related to the motion of fluid particles along relative streamlines fitting to approximately conical surfaces in the vicinity of the blade, as *Figs. 3* and *4* illustrate. The fluid particles move along inward streamlines on the pressure side (PS, *Fig. 3*) and along outward streamlines on the suction side (SS, *Fig. 4*).

In order to establish a simplified 3D blade-to-blade model for the case under investigation, the computed stream traces near the blade surfaces have been approximated as lines fitting to conical patterns able to model the simulated flow behaviour in the core flow region, where the annulus walls and blade edges influence is smoothed (damped). Such modelled conical paths are obtained as lines tangential to the predicted stream traces at their mid-chord radial positions. *Figs. 3* and *4* represent the computed stream traces (solid lines) and their conical approximations (dashed lines) on the PS and SS, respectively.

4. Loading Aspects of Blade-to-Blade Flow

The authors intend to report here a survey on the loading aspects of the 3D interblade flow only for the midspan region (mid-chord radius of $R = 0.84$), for the following

reasons:

1. In the vicinity of the annulus walls, strong over- and underturning flow effects and intense smaller scale 3D vortical flow phenomena appear in the test rotor (CORSINI et al. [4]), thus making doubtful the cascade approach used below.
2. The most intense radial flow occurs near midspan (CORSINI et al. [4]) and thus, the strongest effect of stream surface torsion on rotor loading behaviour is expected here .
3. The appropriateness of CFD simulation is confirmed by experimental data most firmly in the midspan region (best agreement of CFD results with LDA data near midspan, see *Fig. 2*).

4.1. The Approach to Blade-to-Blade Flow Investigation

According to the aims of the investigation, three hypothetical through-flow cases have been considered for present survey. In the first case a hypothetical cylindrical stream tube of $R = 0.84$ is taken through the rotor, according to the design concept. This case is denoted 'Cylinder' later on. The two further cases, suggested by the CFD analysis, assume that the through-flow occurs on conical stream tubes. These two hypothetical cases concern conical through-flow stream tubes (for both sides of the blade) fitting either to the approximate inward or to the outward conical stream traces established for mid-chord radius of $R = 0.84$ on the PS and SS, respectively (marked by dashed lines in *Figs. 3* and *4*). The case for which the inward conical stream tube is considered on both sides of the blade will be denoted 'PS cone' in the following section. For the outward cone, 'SS cone' label will be used. The simultaneous use of 'PS cone' and 'SS cone' models for midspan will be referred to as 'cone couple model'.

Table 2. Input parameters for loading calculation

	R_0	R_3	R_{03}	φ_0	φ_3	φ_{03}	ψ_3	β	φ_{r03}	ℓ/t
Cylinder	0.840	0.840	0.840	0.500	0.530	0.515	0.640	0 °	0	1.236
SS cone	0.800	0.880	0.840	0.510	0.520	0.515	0.700	12.4 °	0.113	1.266
PS cone	0.900	0.780	0.840	0.460	0.520	0.490	0.590	−18.2 °	−0.161	1.299

Details concerning the input data for loading calculations at mid-span on cylindrical and conical through-flow cases have been resumed in *Table2*. Inlet and outlet flow properties were taken in the planes of $-0.06X$ and $1.06X$, respectively. R_0 and R_3 are the radii at which the hypothetical conical stream tubes enter and exit the rotor cascade (according to data in *Figs. 3* and *4*), while R_{03} is the mid-radius of the stream tubes. To be consistent with cascade approach generally used in fan design, pitch-averaged flow data were considered, taken from the inlet boundary conditions at R_0 and from the CFD results at the outlet at R_3, φ_0 and φ_3 are the

pitch-averaged inlet and outlet axial flow coefficients. The measured inlet data are reported in CORSINI et al. [4]. The representative axial flow coefficient φ_{03} is obtained for each stream tube as a mean of pitch-averaged axial flow coefficients at inlet and outlet. This definition is consistent with the 2D cascade concepts widely applied in rotor design. ψ_3 is the pitch-averaged ideal total head rise coefficient at the outlet, with assumption of no pre-swirl. The half-angle of conical stream tubes was calculated as follows:

$$\beta = \tan^{-1} \frac{R_3 - R_0}{X_{\text{mid}}}. \tag{1}$$

In the above relationship X_{mid} is the axial chord at midspan, nondimensionalized by the tip radius ($X_{\text{mid}} = 0.365$).

The representative radial flow coefficient was derived from the following relationship:

$$\varphi_{r03} = \varphi_{03} \tan \beta. \tag{2}$$

Although the blade chord ℓ_{cyl} of the elemental cylindrical rotors was constant with span, the conical stream tubes pass the blade actually along longer chords of $\ell_{\text{cyl}}/\cos\beta$, thus causing modification in the rotor solidities:

$$\ell/t = \frac{\dfrac{\ell_{\text{cyl}}}{r_C}}{2R_{03}\dfrac{\pi}{N}} \frac{1}{\cos\beta}. \tag{3}$$

4.2. Blade Pressure Distribution and Estimation of Lift Coefficients

To study the local loading of a blade on a detailed way, the static pressure distributions have been traced on both the PS and SS for blade sections fitting to the three different hypothetical stream tubes. *Figs.* 5.*a* and 5.*b* show the distributions of static pressure along the blade. In *Figs.* 5.*a* and 5.*b* the static pressure is quoted as a static pressure coefficient, C_p, defined as $C_p = (p - p_{\text{ref}})/0.5\rho u_C^2$, where p is the local static pressure, and p_{ref} is the reference static pressure mean value upstream the rotor.

It is conspicuous in *Figs.* 5.*a* and 5.*b* that although the pressure tracing was carried out fitting to three considerably different hypothetical stream tubes, the static pressure distributions are substantially identical.

The load (lift) of a blade section of elemental dh spanwise length and ℓ chord length can be represented by the lift coefficient:

$$c_\ell = \frac{dF_\ell}{\ell dh \dfrac{\rho}{2} w_\infty^2} = \frac{\overline{p}_{eqPS} - \overline{p}_{eqSS}}{\dfrac{\rho}{2} w_\infty^2}. \tag{4}$$

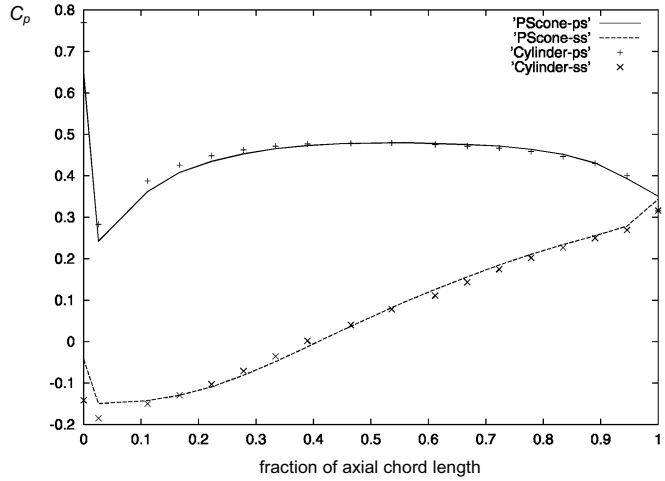

Fig. 5.a. Static pressure distribution about the blade profile near midspan ($R = 0.84$). Comparison between cylindrical and conical (PS cone) pressure distributions

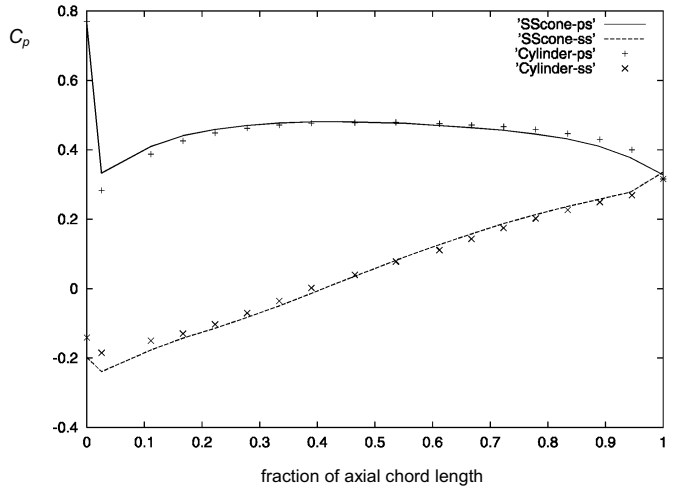

Fig. 5.b. Static pressure distribution about the blade profile near midspan ($R = 0.84$). Comparison between cylindrical and conical (PS cone) pressure distributions

In the above relationship dF_ℓ is the elemental lift force acting on the blade section, ρ is the fluid density and w_∞ is the relative mean velocity along the stream tube. In the above relationship, dF_ℓ is expressed as the difference of representative mean

pressures on the PS and SS ($\overline{p}_{eqPS} - \overline{p}_{eqSS}$), acting on the surface ℓdh. The relative mean velocity (nondimensionalized by the casing relative peripheral velocity u_C) can be calculated using the following relationship:

$$\frac{w_\infty}{u_C} = \sqrt{\varphi_{03}^2 + \varphi_{r03}^2 + \left(R_{03} - \frac{\psi_3}{4R_3}\right)^2}. \tag{5}$$

The w_∞/u_C values calculated on the basis of data summarised in *Table 2* are represented in *Table 3*.

Table 3. Relative mean velocities and calculated lift coefficients

	w_∞/u_C	c_ℓ
Cylinder	0.829	0.744
SS cone	0.830	0.793
PS cone	0.830	0.651

These values are practically equal for the three flow cases. Taking the negligible difference of pressure distributions into account (*Figs. 5.a* and *5.b*) and considering that the direction $\underline{w}_\infty$ of vectors (which is normal to the lift forces) is nearly the same, it is concluded that the $\overline{p}_{eqPS} - \overline{p}_{eqSS}$ representative pressure differences are also nearly equal. The equality of w_∞/u_C and $\overline{p}_{eqPS} - \overline{p}_{eqSS}$ values results in practically equal c_ℓ lift coefficients for the three test cases (see *Eq.* (4)). On the basis of *Figs. 5.a*, *5.b* and taking a dimensionless mean flow velocity $w_\infty/u_C = 0.83$ at midspan, a lift coefficient of $c_\ell = 0.75$ is estimated for each case.

4.3. Pitch-Averaged Flow Analysis

The aim of further investigation was to find a calculation method to point out the equality of the lift coefficients in the three hypothetical flow cases on the basis of cascade approach, i.e. using pitch-averaged flow data. The success of such a method would precipitate that although the interblade stream surfaces are distorted, the loading behaviour of a blade can be suitably described with use of the conical stream tube approach by means of pitch-averaged flow characteristics. The use of pitch-averaged flow data corresponds to a 2D cascade concept, assuming that the series of blade sections bounded by either the SS or the PS conical stream tube segments can be developed into 2D cascade planes.

The loading of the blade for the three flow cases is characterised by use of the following relationship, which is derived from the classic working equation of

an elemental rotor cascade (based on e.g. WALLIS [23]):

$$\frac{\ell}{t}c_\ell \approx \frac{r_3}{r_{03}}\frac{2c_{u3}}{w_\infty} = \frac{R_3}{R_{03}}\frac{\frac{\psi_3}{R_3}}{\frac{w_\infty}{u_C}} \tag{6}$$

with assumption of zero inlet absolute swirl.

From *Eq.* (6), c_ℓ lift coefficients can be calculated for the three flow cases on the basis of pitch-averaged flow data resumed in *Table 2* and the w_∞/u_C data in *Table 3*. The calculated c_ℓ data are presented in *Table 3*. The lift coefficient obtained for the cylindrical stream tube is close to the value assumed theoretically in design for $R = 0.84$ ($c_\ell = 0.749$). The relative difference between lift coefficients established for the conical stream tubes and for the cylindrical one is less than 15 percent. This difference is mainly related to an over-estimation of radial flow effects in the calculation. (The CFD results have not actually reached as high absolute values of radial velocity as considered for φ_{03} in *Table 2*). The mean value of lift coefficients for the two conical stream surfaces is 0.722, approaching well the value of 0.744 for the cylindrical stream tube.

The good agreement of the three calculated c_ℓ values in *Table 3* is in harmony with the previous conclusion stating that the lifts are nearly identical considering the equality of w_∞/u_C and $\overline{p}_{eqPS} - \overline{p}_{eqSS}$ values (see *Eq.* (4)). So it is concluded that with use of pitch-averaged flow data (from *Table 2*) and *Eq.* (6), the lift coefficients can be approached on a satisfactory level for blade sections fitting to conical stream tubes including stream traces separately on PS and SS. Such approach is suggested in spite of the fact that the actual interblade stream surface segments do not fit to axisymmetric tubes but are distorted.

5. Blade Loading Optimisation

As a next step in this train of thoughts, it is assumed that loading behaviour of the blade SS and PS can be characterised separately with use of pitch-averaged data. The reasonableness of this assumption for present case study is supported by the analysis reported in the previous section, suggesting that the blade load related to pressure distribution for non-cylindrical blade sections can be suitably represented using *Eq.* (6) involving pitch-averaged data. As an abstraction, it is assumed that the 'PS cone' approach represents separately the PS load condition, and the 'SS cone' approach represents separately the SS load. The PS contribution to blade loading (according to PS pressure distribution) is approached as if the through-flow would occur at midspan along a conical stream tube fitting to the inward stream trace in *Fig. 3* ('PS cone'). Similarly, the SS loading is approached using an outward conical stream tube model as illustrated in *Fig. 4* ('SS cone'). The synthetic cone couple model for blade loading considers load contribution according only to the SS pressure distribution from the 'SS cone' approach and only the PS pressure

distribution from the 'PS cone' approach. The cones can be transformed into 2D cascade planes. According to the above hypothesis, the optimisation of the blading can be carried out separately for the PS and SS using 2D cascade concepts utilising pitch-averaged flow data. A possible starting point of such two-side ('cone couple') optimisation is to establish optimum lift coefficients separately for both PS and SS. To be consistent with the original design method of the test rotor, the same blade load optimisation method will be applied to the cone couple model. Accordingly, the classic relationship by HOWELL [8] is used, proposed for determination of optimum lift coefficient on the basis of 2D stationary cascade measurement data:

$$c_\ell^* = 2\left(\frac{\cos\alpha_0}{\cos\alpha_3}\right)^{2.75}. \tag{7}$$

The inlet and outlet flow angles are derived as follows:

$$\alpha_0 = \tan^{-1}\frac{R_0}{\varphi_{03}/\cos\beta}, \tag{8}$$

$$\alpha_3 = \tan^{-1}\frac{R_3 - (\psi_3/2R_3)}{\varphi_{03}/\cos\beta}. \tag{9}$$

Table 4. Flow angles and optimum lift coefficients

	α_0	α_3	c_ℓ^*
Cylinder	58.5°	41.7°	0.749
SS cone	56.6°	42.4°	0.892
PS cone	60.2°	37.9°	0.561

Table 4 presents the flow angles and the optimum lift coefficients according to *Eq.* (7), calculated for the different through-flow cases, using the data in *Table2*. As data in *Table 4* indicate, the optimum lift coefficients for SS and PS differ considerably from the value derived for the cylindrical stream tube. This fact anticipates that a separate geometrical optimisation of the blade SS and PS is essential if the 3D blade-to-blade flow is intended to be considered properly in NFV fan design with use of 2D cascade data. Namely, the geometry of blade must accommodate simultaneously different conical through-flow conditions near the blade SS and PS. This means that the sloping blade sections fitting to the SS and PS through-flow cones must fulfil different geometrical demands. Such different but parallel demands can be prescribed through a two-side optimisation using 2D cascade data, as outlined in a following paper (VAD et al. [22]).

6. Conclusions

The 3D interblade flow has been investigated in a CFD case study of axial flow fan rotor of non-free vortex design. A model has been outlined for the 3D blade-to-blade flow. On the basis of this model, the blade loading aspects of 3D flow have been studied using pitch-averaged flow calculations and static pressure distribution maps. The results of present case study are summarised as follows:

1. The interblade stream surface segments were found distorted due to non-free vortex operation, behaving as expected. The streamlines in the vicinity of the blades have been modelled fitting to outward and inward conical stream tubes on the blade suction and pressure sides, respectively – termed 'cone couple model'.
2. It has been pointed out that the blade lift can be satisfactorily described at midspan in a synthesised manner, with concerted utilisation of outward (suction side) and inward (pressure side) conical stream tube models and application of pitch-averaged flow data for the cone couple.
3. Sample calculations have been carried out for determination of optimum lift coefficients at midspan separately for the blade suction and pressure sides, on the basis of the cone couple model and utilisation of 2D stationary cascade measurement data. The results suggested that separate optimisation of the blade suction and pressure side geometry is essential if the 3D blade-to-blade flow is intended to be considered in NFV fan design with use of 2D cascade data.

Acknowledgement

Hungarian authors (J. Vad, F. Bencze) acknowledge the support of OTKA (Hungarian National Foundation for Science and Research) under contract T 025361 and of the Hungarian Ministry for Education under contract FKFP 0356/1999. On behalf of author J. Vad, the research activity documented in this paper is also supported by the János Bolyai Hungarian National Research Grant, Ref. No. BO/00150/98. Italian authors (A. Corsini, F. Rispoli) acknowledge the support of MURST under contract 2539/98. The concerted research activity has been carried out within the framework of Hungarian-Italian Intergovernmental R&D (TéT) Cooperation Project I-28/98.

List of Symbols

c	absolute velocity
c_ℓ	lift coefficient
C_p	pressure coefficient
ℓ	blade chord

N	blade number
p	static pressure
r	radius
PS, SS	pressure side, suction side
$R = r/r_C$	dimensionless radius
$t = 2r\pi/N$	blade pitch
u_C	reference velocity ($r_C \cdot \omega$)
w_∞	relative mean velocity
X	axial chord at hub
α	flow angle (measured from the axial direction)
β	conical stream surface half-angle
Φ_D	flow coefficient (area-averaged axial velocity in the annulus divided by u_C)
$\varphi = c_x/u_C$	pitch-averaged axial flow coefficient
$\varphi_r = c_r/u_C$	pitch-averaged radial flow coefficient
$\psi_3 = 2Rc_{3u}/u_C$	pitch-averaged ideal total head rise coefficient (assuming zero inlet swirl)
Ψ	average total head rise coefficient (total head rise in the annulus normalised by $\rho u_C^2/2$)
ρ	fluid density
ω	rotor angular speed

Subscripts and Superscripts

C	casing wall, casing radius
cyl	cylindrical
D	design
ref	reference value
r, u, x	radial, tangential, axial
0	rotor inlet plane
03	rotor midplane
3	rotor exit plane
$*$	optimum value

References

[1] BASSON, A. – LAKSHMINARAYANA, B., Numerical Simulation of Tip Clearance Effects in Turbomachinery. *ASME J. Turbomachinery*, (1995), pp. 348–359.

[2] BORELLO, D. – CORSINI, A. – RISPOLI, F., A 3D Stabilized Finite Element Technique with Compact Stiffness Matrix Treatment. Application to Internal Flows. *ASME FEDSM and Fluids Engineering Conference*, Vancouver, 1997.

[3] BROOKS, A. N. – HUGHES, T. J. R., Streamline Upwind/Petrov-Galerkin Formulations for Convection Dominated Flows with Particular Emphasis on the Incompressible Navier-Stokes Equations. *Comp. Meth. Appl. Mech. Eng.*, **32** (1982).

[4] CORSINI, A. – RISPOLI, F. – BENCZE, F. – VAD, J., Concerted Experimental and Numerical Studies on Axial Flow Fan Rotor Aerodynamics. *Proc. 3rd European Conference on Turbomachinery, Fluid Dynamics and Thermodynamics*, 1999, London, United Kingdom, (1999), pp. 519–531.
[5] DRING, R. P. – JOSLYN, H. D. – HARDIN, L. W., An Investigation of Axial Compressor Rotor Aerodynamics. *ASME Journal of Engineering for Power*, **104** (1982), pp. 84–96.
[6] GOYAL, R. K. – DAWES, W. N., A Comparison of the Measured and Predicted Flow Field in a Modern By-pass Configuration. *ASME J. of Turbomachinery*, (1993), pp. 273–282.
[7] HAH, C., A Numerical Modelling of Endwall and Tip-clearance Flow of an Isolated Compressor Rotor. *ASME J. of Eng. For Power*, (1986), pp. 15–21.
[8] HOWELL, A. R., The Present Basis of Axial Flow Compressor Design, Part 1: Cascade Theory and Performance. *Aeronautic Research Council R and M 2095*, 1942.
[9] HORLOCK, J. H. – MARSH, H., Flow Models for Turbomachines. *J. Mech. Eng. Sci.*, **13** (1971).
[10] KUNZ, B. – LAKSHMINARAYANA, B., Three-dimensional Navier-Stokes Computation of Turbomachinery Flows Using an Explicit Numerical Procedure and a Coupled $k - e$ Turbulence Model. *J. of Turbomachinery*, **114** (1992), pp. 627–642.
[11] LAKSHMINARAYANA, B., Fluid Dynamics and Heat Transfer of Turbomachinery, John Wiley & Sons, Inc. 1996.
[12] LAUNDER, B. E., Advanced Turbulence Models for Industrial Applications, *Turbulence and Transition Modelling - ERCOFTAC/IUTAM*, (1995), pp. 193–231.
[13] RISPOLI, F. – SICILIANI, F., Una metodologia agli elementi finiti per il calcolo dei flussi secondari incompressibili in condotti di turbomacchine (in Italian), 49^{h} *ATI National Conference*, (1994), pp. 1795–1807.
[14] SAAD, Y. – SCHULTZ, M. H., GMRES: a Generalized Minimal Residual Algorithm for Solving Nonsymmetric Linear System. *SIAM J. of Stat. Comput.*, **7** (1986), pp. 856–869.
[15] SOMLYÓDY, L., Berechnung der Beschaufelung und der Strömung axial durchströmter Wirbelmaschinen mit Anwendung von Gittermessung. *Periodica Polytechnica*, No. 3. Budapest, 1971.
[16] STORER, J. A. – CUMPSTY, N. A., Tip Leakage Flow in Axial Compressors. *ASME J. of Turbomachinery*, (1991), pp. 252–259.
[17] TEZDUYAR, T. E., Stabilised Finite Element Formulations for Incompressible Flow Computations. *Advances in Applied Mechanics*, Academic Press Inc., 1992.
[18] VAD, J. – BENCZE, F. – CORSINI, A. – RISPOLI, F., Three-Dimensional Flow Development Inside an Axial Flow Fan of Non-Free Vortex Design, *Proc. 11th Conference on Fluid and Heat Machinery and Equipment*, September 1999, Budapest, Hungary.
[19] VAD, J. – CSONKA, SZ. – BENCZE, F., Experimental and Numerical Investigation of Axial Flow Rotor Inlet Condition. *MICROCAD'99 Conference*, 1999, Miskolc, Hungary.
[20] VAD, J. – BENCZE, F., Three-Dimensional Flow in Axial Flow Fans of Non-Free Vortex Design. *International Journal of Heat and Fluid Flow*, **19**, December 1998, pp. 601–607.
[21] VAD, J. – BENCZE, F., Laser Doppler Anemometer Measurements Upstream and Downstream of an Axial Flow Rotor Cascade of Adjustable Stagger. *Proc. 9th Int. Conf. Flow Measurement (FLOMEKO)*, Lund, Sweden, (1998) pp. 579–584.
[22] VAD, J. – BENCZE, F. – CORSINI, A. – RISPOLI, F., Design Aspects of Three-Dimensional Flow in High Performance Axial Flow Ventilating Fans. *Proc. 6th International Symposium on Ventilation for Contaminant Control*. June 2000, Helsinki, Finland, pp. 108–110.
[23] WALLIS, R. A., Axial Flow Fans. Newnes, London, 1961.